Heterogeneous Catalysis

International Edition: DOI: 10.1002/anie.201510201
German Edition: DOI: 10.1002/ange.201510201

Selective Alkane Oxidation by Manganese Oxide: Site Isolation of MnO_x Chains at the Surface of $MnWO_4$ Nanorods

*Xuan Li, Thomas Lunkenbein, Verena Pfeifer, Mateusz Jastak, Pia Kjaer Nielsen, Frank Girgsdies, Axel Knop-Gericke, Frank Rosowski, Robert Schlögl, and Annette Trunschke**

Abstract: *The electronic and structural properties of vanadium-containing phases govern the formation of isolated active sites at the surface of these catalysts for selective alkane oxidation. This concept is not restricted to vanadium oxide. The deliberate use of hydrothermal techniques can turn the typical combustion catalyst manganese oxide into a selective catalyst for oxidative propane dehydrogenation. Nanostructured, crystalline $MnWO_4$ serves as the support that stabilizes a defect-rich MnO_x surface phase. Oxygen defects can be reversibly replenished and depleted at the reaction temperature. Terminating MnO_x zigzag chains on the (010) crystal planes are suspected to bear structurally site-isolated oxygen defects that account for the unexpectedly good performance of the catalyst in propane activation.*

The prospective changes in the raw-material basis of the chemical industry to alternative feedstocks bear new scientific challenges. This concerns, in particular, the area of oxidation catalysis where small saturated hydrocarbon molecules are desired building blocks in value-added processes.[1] The activation of inert C–H bonds in alkanes requires highly active catalysts. Often, high activity entails low selectivity owing to the overoxidation of more reactive intermediates and desired products to CO and CO_2.[2] Vanadium oxide is the material that has been most widely studied for the selective oxidation of hydrocarbons and oxygenates.[3] Surface-sensitive in situ experiments indicate that some well-known selective catalysts that consist of crystalline vanadium-containing phases are terminated by two-dimensional vanadium oxide layers.[4] These layers deviate significantly from the bulk crystal structure in terms of their composition and the vanadium oxidation state. The layers account for dynamic charge transfer between bulk and surface. This is reflected in the gas-phase-dependent response of the work function, the electron affinity, and the surface potential barrier, which was not observed for the less-selective bulk V_2O_5.[4i]

Herein, we conceptually confirm that the selectivity of other unselective oxides, such as manganese oxide, is also tunable by applying an extended site-isolation approach. We present the first example of a vanadium-free analogue that accomplishes the efficient activation of propane by establishing a two-dimensional manganese oxide layer in form of MnO_x chains at the surface of phase-pure, rod-shaped, nanostructured $MnWO_4$ (Figure 1; see also the Supporting Information, Figure S1). The catalyst was prepared by hydrothermal synthesis. A previously reported synthesis procedure,[5] was modified in the current work (as described in the Supporting Information).

The phase purity of the synthesis product was confirmed by Rietveld refinement of the powder X-ray diffractogram (Figure S2) by anisotropic fitting. Transmission electron microscopy (TEM) imaging reveals typical rod-shaped nanoparticles with diameters from 13 to 51 nm (Figure 1 a, b, Figure S3), which is in agreement with the XRD analysis (Table S1). Fast Fourier transform (FFT) analysis of the bright-field TEM images of several particles (Figure S4) indicates the preferential growth of the rods along the [001] direction, which is in contrast to a previous report.[5] Furthermore, a power spectrum (Figure 1 b, inset) reveals elongated spots, in particular for the (011) plane, indicating a defective structure. Inverse fast Fourier transformation (IFFT) of the 011 spots (Figure S5) indicates the presence of planar defects within the lattice. From the basal area of two condensed nanorods (Figure 1 c), surface terminations that include the (010), (110), and (100) planes can be distinguished. Atomic-resolution high-angle annular dark field/scanning transmission electron microscopy (HAADF-STEM) images (Figure 1 d and e) viewed along the [001] axis indicate the presence of two kinds of atomic dumbbells, which can be distinguished by their different contrasts. In HAADF-STEM, the contrast is due to Rutherford scattering, which is approximately proportional to Z^2. Therefore, the dumbbells can be attributed to W_2O_8 (high contrast) and Mn_2O_y (low contrast) dimers. In the schematic representation of the $MnWO_4$ crystal structure (Figure 1 f), the W_2O_8 and Mn_2O_y dimers are shown as orange and white edge-sharing octahedra, respectively.

Atomic-resolution HAADF-STEM images of the surface structure of the (010) plane viewed along the [001] direction illustrate the preferential surface exposure of Mn ions as unimers or dimers (Figure 2). The images indicate a slight out-

[*] X. Li, Dr. T. Lunkenbein, V. Pfeifer, M. Jastak, P. K. Nielsen, Dr. F. Girgsdies, Dr. A. Knop-Gericke, Prof. Dr. R. Schlögl, Dr. A. Trunschke
Department of Inorganic Chemistry
Fritz-Haber-Institut der Max-Planck-Gesellschaft
Faradayweg 4–6, 14195 Berlin (Germany)
E-mail: trunschke@fhi-berlin.mpg.de
X. Li, Dr. F. Rosowski
BasCat—UniCat BASF Joint Lab
Technische Universität Berlin
Sekretariat EW K 01, Hardenbergstrasse 36, 10623 Berlin (Germany)
Dr. F. Rosowski
BASF SE, Process Research and Chemical Engineering
Heterogeneous Catalysis
Carl-Bosch-Strasse 38, 67056 Ludwigshafen (Germany)

Supporting information for this article can be found under http://dx.doi.org/10.1002/anie.201510201.

 © 2016 Wiley-VCH Verlag GmbH & Co. KGaA, Weinheim

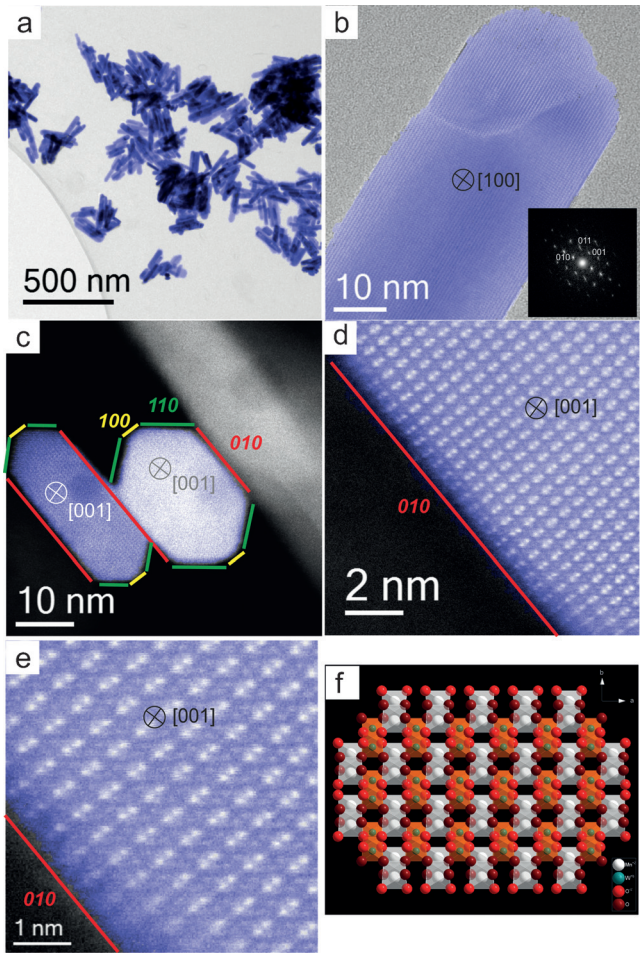

Figure 1. (S)TEM analysis of the $MnWO_4$ powder catalyst. a) Overview TEM image of the $MnWO_4$ nanorods. b) HRTEM image of one nanorod particle viewed along the [100] direction. The inset shows the power spectra recorded on either side of the defect. c) HAADF-STEM image of condensed [001] oriented $MnWO_4$ nanorods. The surface termination was identified by phase analysis of the corresponding atomic-resolution HAADF-STEM images. d), e) Atomic-resolution HAADF-STEM images of (c). f) Schematic representation of the crystal structure of $MnWO_4$ viewed along the [001] direction. Mn white, O red, W green. The original images are shown in the Supporting Information (Figure S1, 6c).

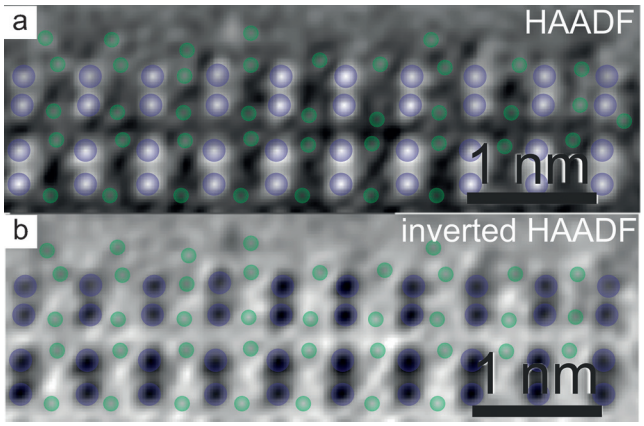

Figure 2. Surface termination of the *b* plane viewed along the growth direction [001] by FFT-filtered atomic-resolution STEM images. a) HAADF, and b) inverted HAADF image. Mn green, W violet. The micrographs correspond to the magnified images of Figure 1d. The original images are given in the Supporting Information (Figure S6).

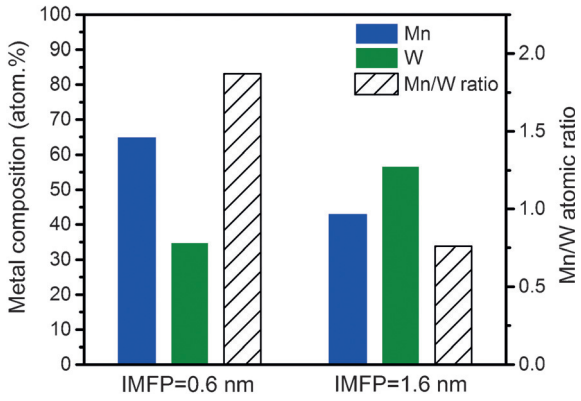

Figure 3. Depth profile of the elemental composition of $MnWO_4$ nanorods at two different depths in terms of the inelastic mean free path (IMFP) of electrons measured by synchrotron-based NAP-XPS at $T = 300\,°C$ applying a total pressure of 0.25 mbar O_2 and He at flows of 2 and 2.2 mL min^{-1}, respectively.

of-center shift for some Mn ions relative to their bulk crystallographic position.

The Raman spectrum of nanostructured $MnWO_4$ agrees well with the spectrum of crystalline $MnWO_4$ (Figure S7).[6] However, two additional, previously unreported bands appear at 615 and 665 cm^{-1}. As the phase purity and high crystallinity of the nanostructured material had been confirmed by TEM (Figure 1 and Figure S8) and XRD (Figure S2), these two bands were attributed to the MnO_x clusters at the surface of the nanorods (Figure S9), which had been visualized by STEM (Figure 2).[7]

Synchrotron-based near-ambient-pressure X-ray photoelectron spectroscopy (NAP-XPS) displays a molar Mn/W ratio of 1.9 (Figure 3), which thus reveals an enrichment of Mn in the outermost surface (inelastic mean free path (IMFP) = 0.6 nm).

In summary, an enrichment of the surface of $MnWO_4$ nanorods with manganese in the phase-pure, highly crystalline material was indicated by photoelectron spectroscopy. The specific surface termination is also reflected in the Raman spectrum. In line with these integral methods, locally resolved atomic-resolution HAADF-STEM images reveal partial Mn surface termination of the (010) planes (Figure 2). Therefore, the Mn enrichment observed by integral methods could be primarily due to an increased occurrence of Mn-terminated (010) planes in the nanostructured material (Figure 2).

The specific surface/nanostructure of $MnWO_4$ is generated under hydrothermal conditions. In situ Raman spectra taken during the synthesis (Figure 4) provide important information on the phase formation of $MnWO_4$. The $MnWO_4$ nanorods develop at around 125 °C when a mixture of aqueous solutions of Na_2WO_4 and $Mn(NO_3)_2$ is heated in an autoclave (Figure S10). The transformation of an intermediate (910 cm^{-1}) into crystalline $MnWO_4$ is indicated by

 © 2016 Wiley-VCH Verlag GmbH & Co. KGaA, Weinheim

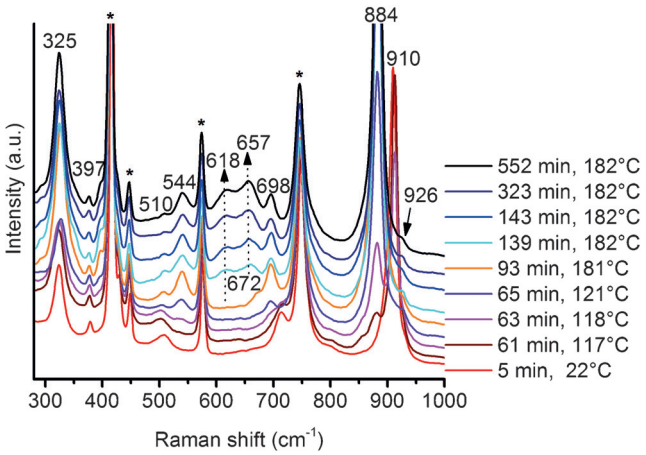

Figure 4. In situ Raman spectra (280–1000 cm^{-1}) recorded during the hydrothermal synthesis of $MnWO_4$ nanorods. Bands denoted with asterisks belong to the sapphire window of the Raman probe.

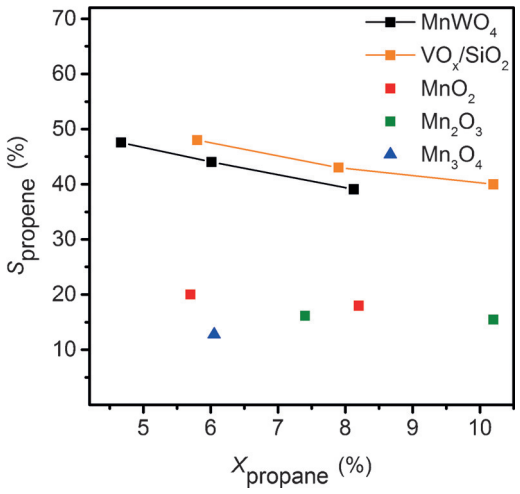

Figure 5. Catalytic performance of nanostructured $MnWO_4$ ($T = 400\,°C$, $W/F = 1.8–0.9\ g\,s\,mL^{-1}$) in comparison to VO_x/SiO_2 ($T = 400–420\,°C$, $W/F = 1.8\ g\,s\,mL^{-1}$) and various manganese oxides ($T = 330–395\,°C$, $W/F = 1.8\ g\,s\,mL^{-1}$) in the oxidative dehydrogenation of propane in a $C_3H_8/O_2/N_2$ feed (10:5:85). The selectivity to propene is shown as a function of propane conversion. Other carbon-containing products are mainly CO and CO_2.

the appearance of bands at 884, 325, 397, 510, 544, 672, and 698 cm^{-1}. The strongest band at 884 cm^{-1} has been assigned to the stretching mode of W=O in distorted WO_6 octahedra.[6] Interestingly, two new bands at 618 and 657 cm^{-1}, which were assigned to surface MnO_x clusters,[7] increase in intensity with time once a synthesis temperature of 180 °C has been reached. $MnWO_4$ crystallizes in a monoclinic structure (wolframite-type, ICSD-67906) in which WO_6 clusters form zigzag chains by sharing edges along the [001] axis (Figure S9). In basic medium under hydrothermal conditions (pH 9), WO_x clusters on the surface of the (010) planes could be dissolved by nucleophilic attack of OH^- ions at the bridging W–O–W bonds [Eq. (1)], leaving behind leached (010) surfaces composed of MnO_x zigzag chains. Subsequently, the bridging oxygen anions at the (001) surface may condense with the dissolved WO_4^{2-} monomers (shoulder at 926 cm^{-1} in Figure 4). Hence, the zigzag chains will propagate in one dimension by forming new O–W–O bridging bonds by edge sharing. Such a dissolution–recrystallization process may result in the observed anisotropic crystal growth along the [001] axis, resulting in the rod-shaped morphology of the $MnWO_4$ particles with a MnO_x enriched surface.

$$MnWO_4 + 2\,OH^- \rightleftharpoons Mn(OH)_2 + WO_4^{2-} \quad (1)$$

The nanostructured $MnWO_4$ material was studied as a catalyst in the oxidative dehydrogenation of propane. Conventional crystalline bulk $MnWO_4$ is rather inactive in the reaction, which is reflected in no measurable conversion at 450 °C. Nanostructuring, however, as achieved by hydrothermal synthesis in the present work, can turn this material into an active catalyst with a similar performance to silica-supported vanadium oxide (Figure 5). Moreover, the unique surface structure of the $MnWO_4$ nanorods leads to superior selectivity to the desired product propylene compared with bulk manganese oxide. Manganese oxide is very active (Table 1), but not very selective and transforms propane almost completely into carbon oxides. The electronic modification and/or the geometric separation of the MnO_x zigzag chains on the (010) planes by W_2O_8 units (Figure 2) apparently account for the improved performance. The propane conversion can be changed by varying the contact time at 400 °C (Figure 5). The comparatively low temperature was chosen to avoid the influence of homogeneous gas-phase reactions, which normally contribute to non-negligible conversion at elevated reaction temperatures above 450 °C. The catalytic performance of the $MnWO_4$ nanorods reached a steady state after 70 hours on stream and showed no signs of deactivation within 108 hours (Figure S11). Importantly, the Mn-terminated $MnWO_4$ nanorods exhibit a much higher apparent turnover frequency (TOF) than silica-supported vanadium oxide species (Table 1) when all Mn atoms at the (010) surfaces and all V atoms are considered to be active sites. However, in reality, the number of active sites at the surface of the catalysts might be much lower.

Table 1: Active-site density and reactivity of the catalysts in the oxidative dehydrogenation of propane at $T = 400\,°C$ and $W/F = 1.8\ g\,s\,mL^{-1}$ in a $C_3H_8/O_2/N_2$ feed (10:5:85).

Catalyst	$MnWO_4$ nanorods	Acid-washed $MnWO_4$[a]	VO_x/SiO_2[b]	Mn_2O_3
rC_3H_8 [$\times 10^{-9}$ mol $m^{-2}\,s^{-1}$]	8.69	2.46	0.27	550
Active-site density [nm^{-2}]	8.3[c]/3[d]	–	1.0	10.2[e]
TOF [$\times 10^{-3}\ s^{-1}$]	0.63/1.7	–	0.16	33

[a] Treatment described in the Supporting Information. [b] VO_x supported on modified SBA-15 with a surface vanadium density of 1 V atom/nm^2. [c] Assuming that only MnO_x species on (010) surface planes are active. [d] Assuming that only oxygen defect sites on the surface are active sites. [e] Mn density on the (100) plane.

© 2016 Wiley-VCH Verlag GmbH & Co. KGaA, Weinheim

The Mn 2p XPS spectra (Figure S12) indicate that Mn is predominantly present in the +2 oxidation state at the surface and within the subsurface. Tiny differences were observed in spectra recorded under different reaction atmospheres (Figure S13); however, the interpretation of the Mn 2p spectra is not straightforward owing to less distinct variations in the binding energies of compounds containing Mn in different oxidation states, elaborate multiplet splitting, and the appearance of satellites.[8] In contrast, near-edge X-ray absorption fine structure (NEXAFS) spectroscopy is sensitive enough to detect the surface oxidation state of manganese oxides[9] and changes in the coordination environment of the Mn ions.[10] The measured line shape of the Mn $L_{2,3}$ edge (Figure S14) agrees well with those found for large single crystals of $MnWO_4$.[11] The spectra confirm the predominance of Mn in the +2 oxidation state both in oxygen and reaction atmosphere. Nevertheless, a small increase in the intensity ratio of the peaks at 640.0 and 641.4 eV was observed during the reaction (Table S2). With increasing oxidation state or, in other words, with increasing coordination of the Mn ions by oxygen atoms, the intensity in the Mn $L_{2,3}$ edge spectrum is shifted towards higher energies.[9] Hence, the changes in the intensity ratio of the peaks at 640.0 and 641.4 eV indicate that the concentration of oxygen defects is higher in the reaction feed than under oxygen atmosphere, suggesting that the oxygen defects have a substantial impact on the catalyst performance. The oxygen defects were quantified by two temperature-programmed oxidation (TPO) and reduction (TPR) cycles (Figure S15). Before the first TPO run, the catalyst was heated in argon atmosphere at 400 °C for two hours. Approximately three oxygen atoms per nm^2 could be replenished after this treatment (Table S3). This result underlines the notion[12] that only a fraction of the surface atoms is catalytically active, which, however, holds great challenges in terms of the identification of active sites. The very similar hydrogen-consumption profiles of the two TPR runs indicate that approximately 5% of the surface oxygen atoms were reversibly removed by reacting with H_2 (Table S3).

After washing the catalyst with nitric acid solution and recalcination under the same conditions as those used for the pristine $MnWO_4$ nanorods, the catalytic activity decreased dramatically (Table 1). Only Mn was detected in the washing solution (Table S4). This further corroborates our argument that surface MnO_x chains are the active sites of the nanostructured $MnWO_4$ catalyst in the oxidative dehydrogenation of propane.

In summary, we have demonstrated that a catalytically inactive solid, such as $MnWO_4$, can be converted into a highly active and selective catalyst by knowledge-based synthesis. Hydrothermal techniques guided by in situ spectroscopy[13] were applied to control the surface termination. In situ Raman spectroscopy provided insight into the molecular processes of crystallization, surface dissolution, and recrystallization under hydrothermal conditions. The unique self-supported structure of the one-dimensional MnO_x clusters at the surface of nanostructured $MnWO_4$ demonstrates the importance of understanding synthetic inorganic chemistry from a molecular point of view[14] and the significance of studying the surface termination[4d,e,15] of well-defined nanostructured metal oxides.[16] The identification of the highly active surface MnO_x units on the $MnWO_4$ nanorods improves our understanding of the promotional effect of Mn in many catalytic systems. The design of selective oxidation catalysts will benefit from this knowledge, which will also enable the improvement of current manganese-doped catalytic systems.

Experimental Section

The hydrothermal synthesis and the thermal activation procedures of $MnWO_4$ are described in in the Supporting Information. In situ Raman measurements were performed with a Kaiser Optics Raman spectrometer RXN1 equipped with a fiber-optic probe head at a laser wavelength of 785 nm. Additional experimental details of the characterization techniques and catalytic tests are summarized in the Supporting Information.

Acknowledgements

This work was conducted in the framework of the BasCat collaboration between BASF SE, TU Berlin, FHI, and the cluster of excellence "Unified Concepts in Catalysis" (UniCat, www.unicat.tu-berlin.de). X.L. acknowledges the Berlin International Graduate School of Natural Sciences and Engineering (BIG NSE) for financial support. We thank Maike Hashagen, Jasmin Allan, Achim Klein-Hoffmann, Dr. Olaf Timpe, and Caroline Dessal for technical assistance. We thank the HZB staff for their continuous support of the electron spectroscopy activities of the FHI at BESSY II.

Keywords: heterogeneous catalysis · hydrothermal synthesis · in situ Raman spectroscopy · manganese tungstate · oxidative dehydrogenation

How to cite: *Angew. Chem. Int. Ed.* **2016**, *55*, 4092–4096
Angew. Chem. **2016**, *128*, 4161–4165

[1] R. Schlögl, *Top. Catal.* **2011**, *54*, 627–638.
[2] F. Cavani, N. Ballarini, A. Cericola, *Catal. Today* **2007**, *127*, 113–131.
[3] a) C. A. Carrero, R. Schloegl, I. E. Wachs, R. Schomaecker, *ACS Catal.* **2014**, *4*, 3357–3380; b) K. Chen, A. Khodakov, J. Yang, A. T. Bell, E. Iglesia, *J. Catal.* **1999**, *186*, 325–333; c) K. Chen, E. Iglesia, A. T. Bell, *J. Catal.* **2000**, *192*, 197–203; d) T. Blasco, J. M. L. Nieto, *Appl. Catal. A* **1997**, *157*, 117–142; e) C. Hess, *ChemPhysChem* **2009**, *10*, 319–326; f) I. E. Wachs, *Dalton Trans.* **2013**, *42*, 11762–11769; g) B. M. Weckhuysen, D. E. Keller, *Catal. Today* **2003**, *78*, 25–46.
[4] a) M. Hävecker, R. W. Mayer, A. Knop-Gericke, H. Bluhm, E. Kleimenov, A. Liskowski, D. Su, R. Follath, F. G. Requejo, D. F. Ogletree, M. Salmeron, J. A. Lopez-Sanchez, J. K. Bartley, G. J. Hutchings, R. Schlögl, *J. Phys. Chem. A* **2003**, *107*, 4587–4596; b) M. Hävecker, A. Knop-Gericke, H. Bluhm, E. Kleimenov, R. W. Mayer, M. Fait, R. Schlögl, *Appl. Surf. Sci.* **2004**, *230*, 272–282; c) E. Kleimenov, H. Bluhm, M. Hävecker, A. Knop-Gericke, A. Pestryakov, D. Teschner, J. A. Lopez-Sanchez, J. K. Bartley, G. J. Hutchings, R. Schlögl, *Surf. Sci.* **2005**, *575*, 181–188; d) A. C. Sanfiz, T. W. Hansen, D. Teschner, P. Schnörch, F. Girgsdies, A. Trunschke, R. Schlögl, M. H. Looi, S. Bee Abd Hamid, *J. Phys. Chem. C* **2010**, *114*, 1912–1921; e) M. Hävecker, S. Wrabetz, J. Kröhnert, L.-I. Csepei, R. Naumann d'Alnoncourt, Y. V. Kolen'ko, F. Girgsdies, R. Schlögl, A. Trunschke, *J.*

 © 2016 Wiley-VCH Verlag GmbH & Co. KGaA, Weinheim

Catal. **2012**, *285*, 48 – 60; f) M. Eichelbaum, R. Glaum, M. Hävecker, K. Wittich, C. Heine, H. Schwarz, C.-K. Dobner, C. Welker-Nieuwoudt, A. Trunschke, R. Schlögl, *ChemCatChem* **2013**, *5*, 2318 – 2329; g) C. Heine, M. Hävecker, M. Sanchez-Sanchez, A. Trunschke, R. Schlögl, M. Eichelbaum, *J. Phys. Chem. C* **2013**, *117*, 26988 – 26997; h) C. Heine, M. Hävecker, E. Stotz, F. Rosowski, A. Knop-Gericke, A. Trunschke, M. Eichelbaum, R. Schlögl, *J. Phys. Chem. C* **2014**, *118*, 20405 – 20412; i) M. Eichelbaum, M. Hävecker, C. Heine, A. M. Wernbacher, F. Rosowski, A. Trunschke, R. Schlögl, *Angew. Chem. Int. Ed.* **2015**, *54*, 2922 – 2926; *Angew. Chem.* **2015**, *127*, 2965 – 2969; j) C. Heine, M. Hävecker, A. Trunschke, R. Schlögl, M. Eichelbaum, *Phys. Chem. Chem. Phys.* **2015**, *17*, 8983 – 8993.

[5] S.-H. Yu, B. Liu, M.-S. Mo, J.-H. Huang, X.-M. Liu, Y.-T. Qian, *Adv. Funct. Mater.* **2003**, *13*, 639 – 647.

[6] a) L. H. Hoang, N. T. M. Hien, W. S. Choi, Y. S. Lee, K. Taniguchi, T. Arima, S. Yoon, X. B. Chen, I.-S. Yang, *J. Raman Spectrosc.* **2010**, *41*, 1005 – 1010; b) M. N. Iliev, M. M. Gospodinov, A. P. Litvinchuk, *Phys. Rev. B* **2009**, *80*, 212302.

[7] a) F. Kapteijn, A. D. Vanlangeveld, J. A. Moulijn, A. Andreini, M. A. Vuurman, A. M. Turek, J. M. Jehng, I. E. Wachs, *J. Catal.* **1994**, *150*, 94 – 104; b) F. Buciuman, F. Patcas, R. Craciun, D. R. T. Zahn, *Phys. Chem. Chem. Phys.* **1999**, *1*, 185 – 190.

[8] a) A. J. Nelson, J. G. Reynolds, J. W. Roos, *J. Vac. Sci. Technol. A* **2000**, *18*, 1072 – 1076; b) M. C. Biesinger, B. P. Payne, A. P. Grosvenor, L. W. M. Lau, A. R. Gerson, R. S. C. Smart, *Appl. Surf. Sci.* **2011**, *257*, 2717 – 2730.

[9] a) B. Gilbert, B. H. Frazer, A. Belz, P. G. Conrad, K. H. Nealson, D. Haskel, J. C. Lang, G. Srajer, G. De Stasio, *J. Phys. Chem. A* **2003**, *107*, 2839 – 2847; b) R. Qiao, T. Chin, S. J. Harris, S. Yan, W. Yang, *Curr. Appl. Phys.* **2013**, *13*, 544 – 548.

[10] S. P. Cramer, F. M. F. DeGroot, Y. Ma, C. T. Chen, F. Sette, C. A. Kipke, D. M. Eichhorn, M. K. Chan, W. H. Armstrong, *J. Am. Chem. Soc.* **1991**, *113*, 7937 – 7940.

[11] a) N. Hollmann, Z. Hu, T. Willers, L. Bohatý, P. Becker, A. Tanaka, H. H. Hsieh, H. J. Lin, C. T. Chen, L. H. Tjeng, *Phys. Rev. B* **2010**, *82*, 184429; b) K. V. Shanavas, D. Choudhury, I. Dasgupta, S. M. Sharma, D. D. Sarma, *Phys. Rev. B* **2010**, *81*, 212406.

[12] a) K. Amakawa, L. Sun, C. Guo, M. Hävecker, P. Kube, I. E. Wachs, S. Lwin, A. I. Frenkel, A. Patlolla, K. Hermann, R. Schlögl, A. Trunschke, *Angew. Chem. Int. Ed.* **2013**, *52*, 13553 – 13557; *Angew. Chem.* **2013**, *125*, 13796 – 13800; b) R. Schlögl, *Angew. Chem. Int. Ed.* **2015**, *54*, 3465 – 3520; *Angew. Chem.* **2015**, *127*, 3531 – 3589.

[13] M. Sanchez Sanchez, F. Girgsdies, M. Jastak, P. Kube, R. Schlögl, A. Trunschke, *Angew. Chem. Int. Ed.* **2012**, *51*, 7194 – 7197; *Angew. Chem.* **2012**, *124*, 7306 – 7309.

[14] R. Schlögl, S. Bee Abd Hamid, *Angew. Chem. Int. Ed.* **2004**, *43*, 1628 – 1637; *Angew. Chem.* **2004**, *116*, 1656 – 1667.

[15] W. Zhang, A. Trunschke, R. Schlögl, D. Su, *Angew. Chem. Int. Ed.* **2010**, *49*, 6084 – 6089; *Angew. Chem.* **2010**, *122*, 6220 – 6225.

[16] A. Trunschke in *Nanostructured Catalysts: Selective Oxidations*, The Royal Society of Chemistry, London, **2011**, pp. 56 – 95.

Received: November 2, 2015
Published online: February 23, 2016

 © 2016 Wiley-VCH Verlag GmbH & Co. KGaA, Weinheim